J Appl Electrochem (2007) 37:637–642
DOI 10.1007/s10800-007-9294-4

ORIGINAL PAPER

Characterization of (PVDF + $LiFePO_4$) solid polymer electrolyte

Ch. V. Subba Reddy · M. Chen · W. Jin · Q. Y. Zhu · W. Chen · Sun-il Mho

Received: 15 September 2006 / Accepted: 15 January 2007 / Published online: 14 February 2007

Abstract $LiFePO_4$ nanopowders (50 nm) were prepared through a simple hydrothermal process. Poly vinylidene fluoride (PVDF): $LiFePO_4$ complex membranes as solid polymer electrolytes were characterized. X-ray diffraction (XRD) and differential scanning calorimetric (DSC) studies show a decrease in crystalline size and crystallinity of the polymer PVDF with increasing $LiFePO_4$ concentration. Scanning electron micrographs show smaller spherical domains in the dry film with increased $LiFePO_4$ nanopowder content. Impedance measurements suggest that the ionic conductivity of (PVDF + $LiFePO_4$) increases with increased temperature and lithium powder concentration.

Keywords $LiFePO_4$ nanopowder · Thermal stability · Morphology · Ionic conductivity

1 Introduction

Solid polymer electrolyte materials (SPE) are receiving attention, particularly in the field of solid-state ionics owing to their potential applications in advanced ionic devices [1–5] such as high performance batteries, efficient energy conversion by fuel cells, sensors, super capacitors, electro-chromic windows and analog memory devices. SPE have several advantageous over liquid electrolytes, such as good mechanical properties, ease of fabrication as thin films in desirable size and ability to form good electrode–electrolyte contact. PEO-based polymer electrolytes using alkali salts, plasticizers and inorganic fillers have been extensively studied [6–15]. Polymers such as poly (acrylonitrile) (PAN), poly (methyl methacrylate) (PMMA), poly (vinyl chloride) (PVC) and poly (vinylidene fluoride) (PVDF) have been examined as gel-type polymer electrolytes in energy-storage devices [16–23]. Presently, the majority of lithium batteries use some form of gelated PVDF film as a separator between cathode and liquid electrolyte. Modifications of PVDF-based polymer electrolytes were developed by blending with PMMA, PVC and PVAAc [24–28]. The physical properties of polymer electrolytes are largely affected by the molecular arrangement and chemical dynamics of the polymer chains. An understanding of the interplay between molecular structure and the ion transport mechanism is critical to the growth of new polymer electrolyte materials.

In spite of the industrial importance and wide application of gelated PVDF, the ion conduction mechanism remains unresolved. PVDF, which has a strong electron withdrawing function and a unique arrangement, delivers a high dielectric constant ($\varepsilon = 8.4$). This is effective in dissociating lithium salts to generate a large quantity of charge carriers for conduction. It is highly possible that, apart from the diffusion established by a plasticizer such as ethylene carbonate (EC), propylene carbonate (PC), conduction through the swollen PVDF matrix is also highly credible. The objective of this research is to study the

Ch.V. Subba Reddy (✉) · M. Chen · W. Jin · Q. Y. Zhu · W. Chen
Institute of Materials Science and Engineering, Wuhan University of Technology, Wuhan 430070, P.R.China
e-mail: drsreddy2005@yahoo.com

Ch.V. Subba Reddy · S.-i. Mho
Division of Energy Systems Research, Ajou University, Suwon 443-749, Republic of Korea

morphology, structure, miscibility, ionic conductivity and electrochemical performance of a PVDF electrolyte membrane with lithium nanopowders incorporated during film formation.

2 Experimental

$LiFePO_4$ nanopowders were prepared using a rheological phase reaction method followed by a self-assembling process. $LiOH.H_2O$, $FeC_2O_4.2H_2O$ and $NH_4H_2PO_4$ with molar ratio 1.5:1:1 were dissolved in water and stirred for 4 h; the rheological phase slurry was introduced to the Teflon-lined Parr reactor and kept at 180°C for 24 h. The final solution was cooled naturally and filtered three times. The powder was dried at 80°C for 8 h.

Polymer electrolyte films of $LiFePO_4$ complexed PVDF were prepared using a solution-cast technique. N-methyl 1-2 pyrrolidone (NMP) was used as a solvent. The compositions of the polymer complexes were the following: (100-x) PVDF + $xLiFePO_4$, where x (wt%) = 0,5,10 and 15. The mixtures of salt solutions were stirred for 24 h at 60°C for homogenous mixing and cast in polypropylene dishes. The dish solutions were kept at 50°C for a week in an oven. Thick films of 100–200 μm were collected from the dishes and these were vacuum dried thoroughly at 10^{-3} mbar to remove solvent traces. The XRD patterns of the films were determined using a HZG4/B-PC X-ray diffractrometer with CoKα radiation and a graphite monochrometer. The IR spectra were determined using a 60-SXB FTIR spectrophotometer over the range 400–4000 cm^{-1}. For the DSC measurements, a Netzsch STA 409 PC, operating in dynamic mode (heating rate = 10 $Kmin^{-1}$), was employed. Samples of $\approx$ 5 mg weight were placed in sealed aluminium pans. The morphology of the samples was characterized using a JSM-5610LV scanning electron microscope (SEM).

A home made conductivity cell was used to measure the ionic conductivity of the polymer electrolytes as a function of temperature. The ac impedance measurements of the polymer electrolytes were performed using an Agilent 4294A precision impedance analyzer in the range 40–300 kHz and temperature range 298–368 K. The system was thermally equilibrated at each selected temperature for 15 min. The bulk resistance (R_p) determined from the equivalent circuit analysis by using frequency response analyzer (FRA) software. The conductivity values (σ) were calculated from the equation $\sigma = (1/R_p)(t/A)$, where t is the thickness and A is the sample area.

3 Results and discussion

XRD patterns of the pure PVDF and (PVDF + $LiFePO_4$) films are shown in Fig. 1. Sharp diffraction peaks appear at 2θ~18–21° and demonstrate the crystalline forms of PVDF. A small number of differences are observed between the pure PVDF and $LiFePO_4$ nanoparticle PVDF complexed films. The clear and sharp crystalline diffraction peaks in pure PVDF, however, become less prominent in the presence of the nanoparticles. The decrease in intensity of the diffraction peaks with dopant concentration suggests a decrease in both crystalline size and the degree of PVDF crystallinity. Even though PVDF is not an ionomer, the highly depolarized CF bond is capable of forming a weak acid-based complexation with lithium and thus retards the order of crystalline PVDF.

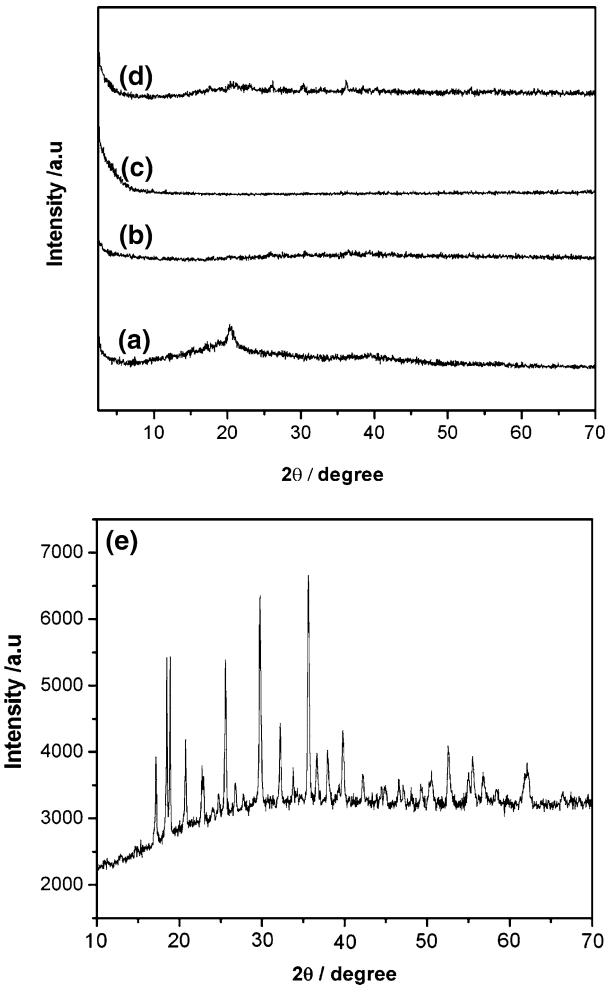

Fig. 1 XRD patterns of (*a*) pure PVDF and $LiFePO_4$ complexed PVDF polymers, (*b*) PVDF + $LiFePO_4$ (95:5), (*c*) PVDF + $LiFePO_4$ (90:10), (*d*) PVDF + $LiFePO_4$ (85:15), (*e*) XRD patterns of pure $LiFePO_4$ nanopowder

Figure 1e shows the XRD patterns of synthesized $LiFePO_4$ nanoparticles. All peaks can be indexed as pure and well-crystallized $LiFePO_4$ phase with an ordered olivine structure and a space group of P_{nma}. The calculated lattice parameters from the XRD data are a = 1.0342 nm, b = 0.6005 nm, and c = 0.4693 nm, which are comparable to the standard data JCPDS 83-2092. The XRD result demonstrates that the rheological self-assembling route can be used to synthesize single-phased $LiFePO_4$ product with no unwanted impurity phases, such as $Li_3PO_4^-$ and Fe^{3+}-related compounds [29]. Conventional solid state methods, although carried out under carefully controlled conditions, have shown the unwanted presence of the impurity phases such as Fe_2O_3 and $Li_3Fe_2(PO_4)_3$ [30]. Another advantage is that the sample can be prepared by this process without sintering. This makes it simple to prepare $LiFePO_4$ olivine materials. In comparison with the previous solid state processes, the rheological self-assembling process reduces the synthesis temperature of $LiFePO_4$. The soft solution environment may remarkably accelerate the reaction kinetics of the formation of $LiFePO_4$.

IR spectra of pure PVDF and (PVDF + $LiFePO_4$) electrolytes of different compositions are shown in Fig. 2a–d. The vibrational peaks of complexed polymer electrolytes are shifted towards higher wave numbers with increasing $LiFePO_4$ concentration. Fig 2e shows IR spectra of $LiFePO_4$ nanoparticles which show the peaks at wavenumbers 3349, 1628, 1371, 1070, 945, 635, 547 and 498 cm^{-1}. The characteristic absorption band of $LiFePO_4$ at 1371 cm^{-1} is associated with the vibration of the P–O–Fe bond in $LiFePO_4$, whereas the bands situated at 1070 and 945 cm^{-1} correspond to the characteristic absorption of the $[PO_4]^{3-}$. The $LiFePO_4$ absorption band between 635 and 547 cm^{-1} is associated with the vibration of P–O bond in $LiFePO_4$. Particularly, the characteristic Li-O absorption band bond at 498 cm^{-1} is weak, which indicates the weak interaction between Li and O atoms, which enables Li^+ ions to insert/extract easily in the ordered olivine $LiFePO_4$ structure [31]. The absence of absorption peaks of pure $LiFePO_4$ nanoparticles in the complexed systems and peak shifts with $LiFePO_4$ concentration indicate the miscibility of the dopant in the prepared electrolyte systems. In addition to the PVDF and $LiFePO_4$ vibrational peaks, some other peaks were observed at the frequencies 1699 and 1450 cm^{-1} and were assigned to CH_3 asymmetric stretching and bending vibrations of PVDF [22]. The appearance of new peaks along with changes in existing peaks in IR spectra indicate directly the complexation of PVDF with $LiFePO_4$.

Differential scanning calorimetry also demonstrated a loss in the long-range order of PVDF in the presence of $LiFePO_4$. DSC curves of pure PVDF and (PVDF + $LiFePO_4$) electrolytes are shown in Fig. 3. Except for pure PVDF, a re-crystallized peak is apparent for all compositions of $LiFePO_4$ complexed PVDF electrolytes during the endothermic reaction. This peak shifts towards lower temperature with increasing dopant content. This behaviour suggests that the additional PVDF crystallization occurs in freshly-prepared (PVDF + $LiFePO_4$) electrolytes upon heating at elevated temperature, possibly by driving the salt out of the amorphous PVDF domain.

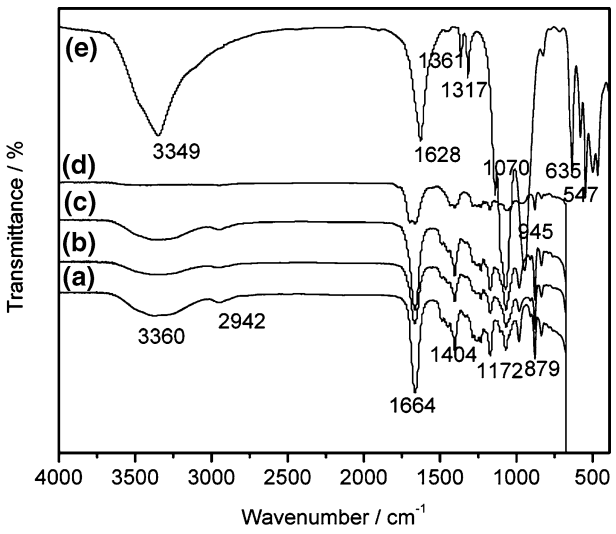

Fig. 2 IR patterns of (*a*) pure PVDF and $LiFePO_4$ complexed PVDF polymers, (*b*) PVDF + $LiFePO_4$ (95:5), (*c*) PVDF + $LiFePO_4$ (90:10), (*d*) PVDF + $LiFePO_4$ (85:15), (*e*) $LiFePO_4$ nanopowder

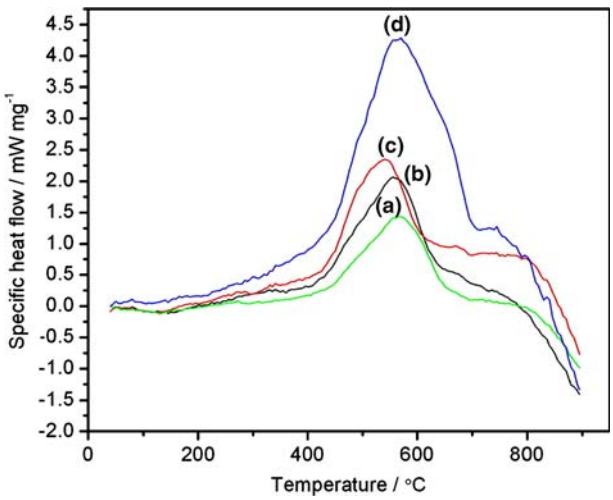

Fig. 3 DSC curves of (*a*) pure PVDF and $LiFePO_4$ complexed PVDF polymers, (*b*) PVDF + $LiFePO_4$ (95:5), (*c*) PVDF + $LiFePO_4$ (90:10), (*d*) PVDF + $LiFePO_4$ (85:15)

Table 1 Melting temperature (T_m), crystallization temperature(T_c), crystallinity (χ), conductivity (σ) and activation energy of (PVDF + $LiFePO_4$) solid polymer electrolytes

$LiFePO_4$ in PVDF/wt%	T_m/°C	T_c/°C	χ/%	Conductivity (at 298 K)/S cm^{-1}	Activation energy /eV
0	570	147	100	2×10^{-6}	0.18 ± 0.04
5	568	129	39.04	2.5×10^{-6}	0.16 ± 0.02
10	557	125	33.2	5.71×10^{-6}	0.12 ± 0.02
15	534	114	29.9	6.66×10^{-6}	0.11 ± 0.03

The heat of fusion (ΔH_f) and the melting temperature (T_m) of polymer PVDF decreases with increasing dopant content. The relative crystallinity (χ) has been determined, by assuming that pure PVDF is 100%, using a formula $\chi = \Delta H_f / \Delta H_f^0$ (where ΔH_f^0 is the fusion heat of pure PVDF and ΔH_f is related to the dopant in the polymer). The crystallinity (χ), melting temperature (T_m) and crystallization temperature (T_c) are listed in Table 1. Polymer electrolytes show lower χ in the presence of lithium ionic nanoparticles.

The TG plots of the (PVDF + $LiFePO_4$) polymer electrolyte system are shown in Fig. 4. The thermal decomposition temperature was determined from the differential curve, and is about 140°C for all (PVDF + $LiFePO_4$) electrolytes. The absence of weight loss prior to polymer melting indicates no impurity, such as solvent or water, is present. Absence of impurity confirms that the vacuum drying is efficient in the present case. The degradation temperature decreases continuously with the increased dopant concentration in the polymer and is directly related to an increase in the amorphous fraction of the electrolyte. The thermal stability of the polymer is reduced with the addition of $LiFePO_4$ due to the growth of the amorphous fraction, which is a characteristic of polymers. A higher fraction of residue is found, at above 500°C, with increased dopant concentration.

SEM photographs of PVDF and (PVDF + $LiFePO_4$) films are shown in Fig. 5a–c. The surface structure of pure PVDF shows connecting big spheres (see Fig. 5a). As PVDF is polymerized with a high dielectric constant, the surface tension is also high. Sol formation is necessary in the process of drying solvent from the miscible solution. The size of the spheres and the morphology in the PVDF film are thus highly

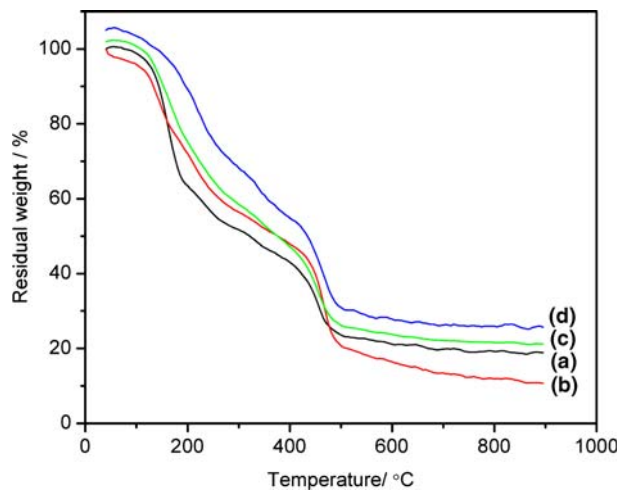

Fig. 4 TG curves of (*a*) pure PVDF and $LiFePO_4$ complexed PVDF polymers, (*b*) PVDF + $LiFePO_4$ (95:5), (*c*) PVDF + $LiFePO_4$ (90:10), (*d*) PVDF + $LiFePO_4$ (85:15)

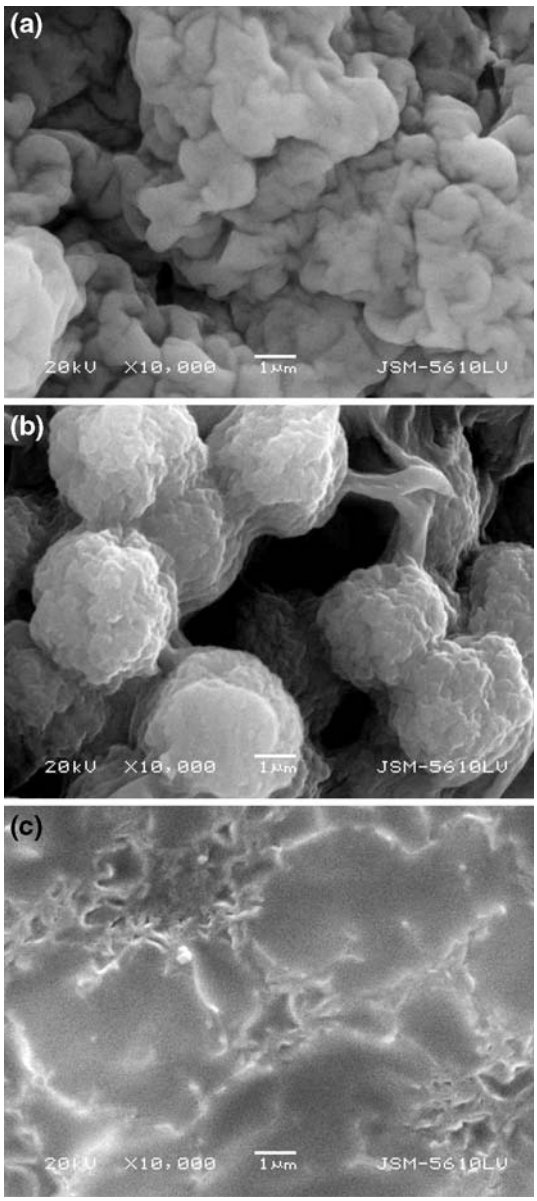

Fig. 5 SEM photographs of (*a*) pure PVDF and $LiFePO_4$ complexed PVDF polymers, (*b*) PVDF + $LiFePO_4$ (95:5), (*c*) PVDF + $LiFePO_4$ (85:15)

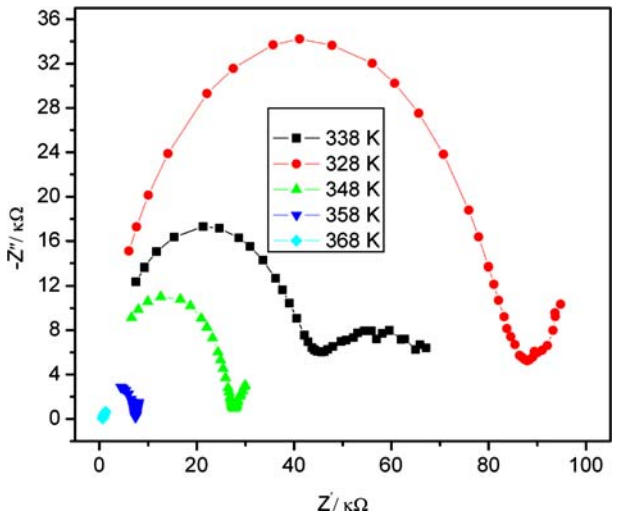

Fig. 6 Impedance plot of pure PVDF at different temperatures

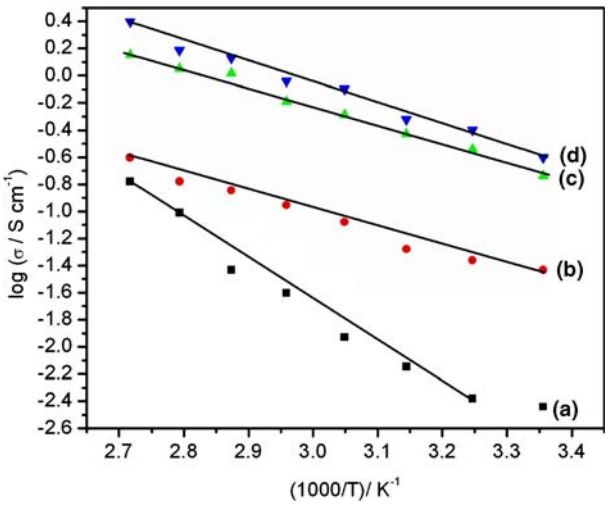

Fig. 7 Temperature dependence conductivity of (*a*) pure PVDF and $LiFePO_4$ complexed PVDF polymers, (*b*) PVDF + $LiFePO_4$ (95:5), (*c*) PVDF + $LiFePO_4$ (90:10), (*d*) PVDF + $LiFePO_4$ (85:15)

dependent on the preparation conditions such as the solvent and the temperature. Addition of $LiFePO_4$ to PVDF, the acid-base interaction, not only changes the crystallinity but also reduces the surface potential and the equilibrium sol dimension becomes smaller. As seen in Fig. 5b, the spheres are converted into a cauliflower shape with improved smoothness. In Fig. 5c, all the spheres are merged together and develop a uniform surface, due to the increasingly amorphous nature of the polymer.

A series of impedance measurements at different temperatures were obtained from 25–95°C. The impedance plots for pure PVDF electrolyte at different temperatures are presented in Fig. 6. Most curves are semicircular in shape with an oblique line. For each curve, the value of R_p was obtained from the intercept point at the high frequency end. The conductivity of the polymer electrolyte was calculated from the measured resistance (R_p), the area and the thickness of the polymer film.

The temperature dependence of conductivity is presented in Fig. 7. Conductivity data at room temperature are noted in Table 1. Interestingly, the conductivity of the complexed PVDF electrolytes increases continuously with $LiFePO_4$ content for all temperatures. This behaviour is different from that of PEO solid polymer electrolyte systems, where a maximum conductivity is identified at a particular compositional ratio [32–36]. In this case, incomplete dissociation and the formation of triplets at higher salt content are responsible for the reduced conductivity. The ion- paring mechanism appears to be absent in the PVDF polymer electrolytes studied, which may be due to the high dielectric constant of the medium.

The plot of logσ versus 1000/T follows an Arrhenius-type thermally-activated process. The conductivity relationship can be expressed as $\sigma = \sigma_0 \exp(-E_a/kT)$, where σ_0 is the pre-exponential factor, E_a is the activation energy and k *is* the Boltzmann constant. Activation energies of (PVDF + $LiFePO_4$) solid polymer electrolytes were evaluated by a linear fitting method; and the results are listed in Table 1. The activation energy decreases with increasing Li ion concentration in the PVDF polymer.

Druger et al. [37, 38] have attributed the change in conductivity with temperature in solid polymer complexed systems to segmental (i.e. polymer chain) motion, which results in an increase in the free volume of the system. Thus, the segmental motion either permits the ions to hop from one site to another or provides a pathway for ions to move. In other words, the segmental movement of the polymer facilitates the transitional ionic motion. From this, it is clear that the ionic motion is due to ionic transitional motion/hopping facilitated by the dynamic segmental motion of the polymer. As the amorphous region increases, however, the polymer chain acquires faster internal modes in which bond rotations produce segmental motion to favor inter- and intra-chain ion hopping and, thus, the degree of conductivity becomes high.

4 Conclusions

The interaction between Li^+ ions and fluorine in the polymer effectively disrupts the crystallinity of PVDF.

The ionic conductivity increases continuously with increased salt concentration. The increased conductivity is due to a decrease in the degree of crystallinity and increase in the amorphous nature of the polymer. The activation energies decrease with increasing dopant concentration.

Acknowledgements One of the authors (Ch.V.S. Reddy) thanks Wuhan University of Technology for the award his Post Doctoral Fellowship and he also thanks Ajou University for the award of his Post Doctoral Fellowship from the BK 21 project. The authors thank Dr. Rajamohan R Kalluru, Mississippi Ethanol LLC, USA for fruitful discussions.

References

1. Armand MB (1986) Ann Rev Mater Sci 16:245
2. Ratner MA, Shriver DF (1988) Chem Rev 88:109
3. Mac Callum JR, Vincent CA (eds.), (1987) Polymer Electrolyte Reviews, Elsevier, Amsterdam
4. Owen JR, Laskar AL, Chandra S (1989) Superionic Solids and Solid State Electrolytes-Recent Trends, Academic Press, New York
5. Murata K (1995) Electrochim Acta 40:2177
6. Reitman EA, Kaplan ML, Kava RJ (1985) Solid State Ionics 17:67
7. Sorensen PR, Jacobson T (1982) Electrochim Acta 27:1675
8. Fautex D, Robitaille C (1986) J Electrochem Soc 133:307
9. Oleksiak AL, Inerowicz HD (1999) J Power Sources 81–82:813
10. Mclin M, Angell CA (1992) Solid State Ionics 56:1027
11. Lee YL, Crist B (1986) J Appl Phys 60:2683
12. Hashmi SA, Chandra A, Chandra S (1992) In: BVR Chowdari, et al. (eds.), Solid State Ionics: Materials and Applications, World Scientific, Singapore :p 567
13. Sreepathi Rao S, Jaipal Reddy M, Laxmi Narsaiah E, Subba Rao UV (1995) Mater Sci Eng B 33:173
14. Sreekanth T, Jaipal Reddy M, Subramanyam S, Subba Rao UV (1999) Mater Sci Eng B 64:107
15. Sreekanth T, Jaipal Reddy M, Ramalingaiah S, Subba Rao UV (1999) J Power Sources 79:105
16. Peramunage D, Pasquariello DM, Abraham KM (1995) J Electrochem Soc 42:1789
17. Hong H, Liquan C, Xujie H, Rongjan X (1992) Electrochim Acta 37:1671
18. Bohke O, Frand C, Razrazi M, Rousselt C, Truche C (1993) Solid State Ionics 66:97
19. Boudin F, Andrieu X, Jehoulet C, Olsen II (1999) J Power Sources 81–82:804
20. Saito Y, Kataoka H, Quartarone E, Mustarelli P (2002) J Phys Chem B 106:7200
21. Saito Y, Kataoka H, Stephan AM (2001) Macromolecules 34:6995
22. Rajendran S, Kannan R Mahendran O (2001) Mater Lett 49:172
23. Subba Reddy ChV, Zhu Quan-Yao, Mai Li-Qiang, Chen Wen J. Solid State.Elect.Chem : In press
24. Moussaif N, Jerome R (1999) Polymer 40:3919
25. Jin Z, Pramoda KP, Goh SH, Xu G (2002) Mater Res Bull 37:271
26. Bauduin G, Boutevin B, Gramain P, Malinova A (1999) Eur Polym J.35:285
27. Rajendran S, Mahendran O Kannan R (2002) Fuel 81:1077
28. Stephan AM, Kumar TP, Renganathan NG, Pitchumani S, Thirunakaran R, Muniyandi N (2000) J Power Sources 89:80
29. Yamada, Chung SC, Hinokuma K (2001) J Electrochem Soc 148:A224
30. Padhi. K, Nanjundaswamy KS, Goodenough JB (1997) J Electrochem Soc 144:1189
31. Chen W, Mai LQ, Xu Q, Zhu QY, Yang HP (2003) Mater Sci Eng B 100:221
32. Chu PP, Jen HP, Lo FR, Lang CL (2000) Macromolecules 32:4738
33. Zahurak SM, Kaplan ML, Rietman EA, Murphy DW, Cava RJ (1988) Macromolecules 21:654
34. Ratner MA, Nitzman A (1989) Faraday Discuss Chem Soc 88:19
35. Dupon R, Papke BL, Ratner MA, Whitmore DH, Shriver DF (1982) J Am Chem Soc 104:6247
36. Reddy MJ, Chu PP (2002) J Power Sources 109:340
37. Druger SD, Nitzam A, Ratner MA (1983) J Chem Phys 79:3133
38. Druger SD, Nitzam A, Ratner MA (1985) Phy Rev B 31:3939